

Voxel-based morphometry indicates relative preservation of the limbic prefrontal cortex in early Huntington disease

M. Mühlau¹, A. Weindl¹, A. M. Wohlschläger^{1,2,3}, C. Gaser⁴, M. Städtler¹, M. Valet¹, C. Zimmer², J. Kassubek⁵, A. Peinemann¹

¹ Department of Neurology, Technische Universität München, Munich, Germany

² Department of Neuroradiology, Technische Universität München, Munich, Germany

³ Department of Nuclear Medicine, Technische Universität München, Munich, Germany

⁴ Department of Psychiatry, University of Jena, Jena, Germany

⁵ Department of Neurology, University of Ulm, Ulm, Germany

Received: June 7, 2006 / Accepted: August 8, 2006 / Published online: October 6, 2006

© Springer-Verlag 2006

Summary In Huntington disease (HD), both the genetic defect and mutant gene product huntington are known but the exact mechanisms that lead to neuronal loss are poorly understood. Until now, the distribution of tissue *loss* throughout the brain has been investigated intensively. Here we searched for areas that, antipodal to the striatum, display grey-matter (GM) preservation. We performed high resolution T1-weighted magnetic resonance imaging and voxel-based morphometry in 46 patients in early HD and 46 healthy controls. We applied an analysis of covariance (ANCOVA) model with the total GM volume of each participant as covariate. In accordance with earlier reports, group comparisons revealed GM decrease in the striatum, insula, and thalamus as well as in dorsolateral frontal and occipital areas. In contrast, the limbic prefrontal cortex displayed GM preservation. Our findings support hypotheses that postulate differential involvement of frontosubcortical circuits in the pathophysiology of HD.

Keywords: Grey-matter preservation, Huntington disease, voxel-based morphometry

Introduction

Huntington disease (HD) is an autosomal dominant neurodegenerative disease. Since the discovery that HD results from an expanded CAG trinucleotide repeat within the IT15 gene located on chromosome 4 (1993), HD has become an attractive model for neurodegeneration. However, the pathomechanisms that lead to the typical distribution of pathological changes throughout the brain (i.e., primarily loss of medium-sized spiny neurons in the striatum)

(Graveland et al., 1985; Vonsattel et al., 1985) and, finally, to the clinical picture of involuntary movements, dementia, and behavioral disturbances are poorly understood. At the molecular level, numerous pathomechanisms triggered by the mutant gene product huntingtin have been discovered and, far from arriving at a unifying mechanism, robust evidence suggests that multiple – probably interacting – pathomechanisms (e.g., glutamatergic excitotoxicity and mitochondrial dysfunction) occur in HD (Gardian and Vecsei, 2004; Leegwater-Kim and Cha, 2004). Moreover, clinical, epidemiological, imaging, and histological studies have provided valuable insights with regard to the severity and variability of clinical symptoms and the involvement of different brain systems.

Perspectively, a comprehensive model of HD must account for multiple pathogenic mechanisms and its interactions and, this way, explain the distribution of pathological changes throughout the brain. Therefore, precise knowledge on the distribution of pathological changes throughout the brain is essential for the understanding of HD. Until now, the distribution of tissue *loss* throughout the brain has been investigated intensively (Kassubek et al., 2004b, 2005; Peinemann et al., 2005; Rosas et al., 2001; Thieben et al., 2002; Vonsattel et al., 1985). In order to further characterize the pattern of grey-matter (GM) changes throughout the brain in HD, we searched for areas that, antipodal to the striatum, display relative preservation of GM or even absolute GM increase. For this purpose, we performed magnetic

Correspondence: Mark Mühlau, MD, Department of Neurology, Technische Universität München, Möhlstrasse 28, 81675 Munich, Germany
e-mail: m.muehlau@neuro.med.tu-muenchen.de

resonance imaging (MRI) and voxel-based morphometry (VBM) in HD patients and healthy controls. VBM enables the detection of subtle structural changes throughout the brain at the group level using MRI. The main idea of VBM comprises the following steps: 1) spatial normalization of all images to a standardized anatomical space to allow averaging; 2) segmentation of images into GM, white matter (WM) as well as cerebrospinal fluid (CSF); and 3) group comparison of GM across the whole brain. This way, both GM decrease and increase can be detected.

Subjects and methods

Subjects

Data and images were derived from routine diagnostics of our HD outpatient clinic that participates in the European Huntington Disease Network (<http://www.euro-hd.net/html/network>) and from healthy volunteers who had participated in other imaging studies at our department. The HD group consisted of 46 gene-positive subjects (woman, 23; left-handers, 2) (Oldfield, 1971) who did not generate motion artifacts during MRI. Seven patients were presymptomatic. Twenty eight patients were in stage I and 11 in stage II according to Shoulson and Fahn (1979). Further details on the HD group are given in the Table 1. Healthy controls were matched for age and sex in a pair-wise manner (woman, 23; left-handers, 2; mean age, 44 years; standard deviation of age, 10).

MRI

Each participant underwent MRI (magnetic field intensity, 1.5 Tesla; scanner, *Siemens Magnetom Symphony*; sequence, T1 magnetization prepared rapid gradient echo (MPRAGE); plane, sagittal; number of slices, 160; slice thickness, 1 mm; voxel size, $1 \times 1 \times 1 \text{ mm}^3$; flip angle, 15° ; field of view, $256 \times 256 \text{ mm}$). After 27 HD patients and 27 controls had undergone MRI (TR, 11.1 ms; TE, 4.3 ms; TI, 800 ms), *Siemens* performed a software upgrade by installing the “*syngo software*” which resulted in slightly different parameters of the standard MPRAGE sequence (TR, 8.9 ms; TE, 3.93 ms; TI, 800 ms). In order to certainly exclude an effect of this software upgrade, the sequence was included in each analysis of covariance (ANCOVA) as additional confounding covariate (see below).

Table 1. Characterization of the HD patients

| | Min | Max | Median | Mean | SD |
|------------------------|-----|-----|--------|------|-----|
| Age ^a | 24 | 68 | 42 | 44 | 11 |
| Onset age ^b | 24 | 62 | 40 | 41 | 10 |
| Time since onset | 0 | 14 | 4.0 | 4.7 | 4.7 |
| MMSE | 18 | 30 | 28 | 27 | 3.0 |
| mUHDRS ^a | 0 | 62 | 13 | 18 | 17 |
| CAG ^c | 40 | 49 | 43 | 44 | 2.4 |

CAG Number of CAG trinucleotide repeats; *Max* maximum; *Min* minimum; *MMSE* mini-mental state examination (Folstein et al., 1975); *mUHDRS* motor score of the Unified HD Rating Scale (1996); *SD* standard deviation. ^a Age correlated significantly with mUHDRS (Spearman correlation coefficient, 0.74; 2-sided *P* value, <0.001). ^b Onset was defined as the occurrence of first motor symptoms. ^c CAG repeats correlated significantly with onset age (Spearman correlation coefficient, -0.52; 2-sided *P* value, 0.002).

Analyses of global volumes

Global volumes of GM, WM, and CSF of each subject were derived from the segmentation process of SPM2. Total intracranial volume (TIV) was defined as the sum of the global volumes of GM, WM, and CSF.

VBM parameters and statistical analyses

SPM2 software (Wellcome Department of Imaging Neuroscience Group, London, UK; <http://www.fil.ion.ucl.ac.uk/spm>) was applied for data processing. VBM was performed according to the “optimized” protocol (Good et al., 2001) using study-specific prior probability maps, the modulation step, and a Gaussian kernel of 8 mm for smoothing. Voxel-by-voxel analysis of covariance (ANCOVA) with MPRAGE-sequence, age, sex, and global GM volume as confounding covariates was used to detect GM differences between both groups.

As a result of nonlinear spatial normalization, the volumes of certain brain regions may grow, whereas others may shrink. Correction for these volume changes by another pre-processing step prior to smoothing has been recommended especially for the investigation of neurodegenerative diseases (Good et al., 2001, 2002). This additional step, the modulation, comprises multiplication of voxel values of the segmented images by the Jacobian determinants. In effect, an analysis of modulated data tests for regional differences in the absolute amount of GM (whereas analysis of unmodulated data tests for regional differences in concentration of GM) (Ashburner and Friston, 2000; Good et al., 2001).

VBM analyses aim to find regionally specific changes that cannot be explained by global effects. Compatible with general brain atrophy, the HD group showed significantly less total GM volume and significantly less total WM volume but significantly more total CSF volume whilst the total intracranial volumes did not differ significantly between both groups (Fig. 1). In order to correct for both brain size and global atrophy, we followed the suggestion of Good et al. (2001, 2002) and included the total GM volume of each participant as covariate in our ANCOVA. In this analysis, areas of GM decrease (in HD compared to controls) display GM loss above average (i.e., significantly less GM than estimated from global atrophy) whilst areas of GM increase display either GM gain or GM preservation (i.e., significantly more GM than estimated from global atrophy) (Good et al., 2001, 2002).

We applied a height threshold of $P < 0.05$ corrected with the family wise error and an extent threshold of $P < 0.05$ corrected (underlying voxel threshold, 0.001) (Friston et al., 1996). To visualize the extension of GM changes, significant clusters are displayed at a voxel threshold of $P < 0.001$.

Moreover, we investigated whether areas of relative GM preservation actually display absolute GM increase. For this purpose, we used the volume of

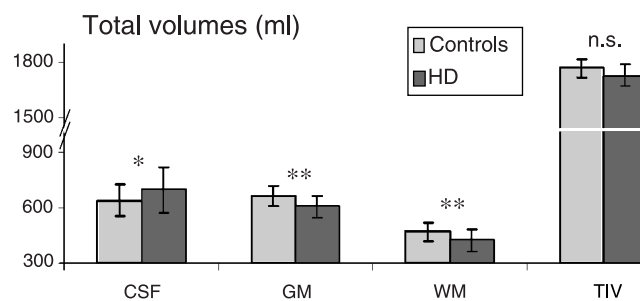


Fig. 1. Total volumes of HD patients and healthy controls. Total volumes of grey and white matter as well as cerebrospinal fluid (GM, WM, CSF) and total intracranial volume (TIV) are shown. Significance of the differences between both groups is indicated (* $P < 0.05$; ** $P < 0.01$; n.s. not significant)

Voxel-based morphometry indicates relative preservation of the limbic prefrontal cortex

interest (VOI) function of SPM2 and extracted the raw values of each cluster (underlying voxel threshold, 0.001). These raw values were orthogonalized to brain size (TIV), sex, and MPRAGE sequence (using a Matlab routine). These orthogonalized data were compared between both groups with *t*-tests.

Finally, we investigated the influence of disease progression on the areas identified by our ANCOVA. In our sample of patients (Table 1), motor impairment significantly correlated with age (Spearman coefficient, 0.74; 2-sided *P* value, <0.001). Since different age-related changes between both groups had to be attributed to the progression of HD, we performed an interaction analysis of age with group. For this purpose, the extracted and orthogonalized values of each cluster (of all 96 participants) were fed in a step wise regression analysis (Statistical Package for the Social Sciences software (SPSS); version, 12.0.1; Chicago, Illinois, USA) as dependent variable. Age, group (controls, -1; HD, 1) and the interaction of age and group (product of age and group) served as independent variables.

Voxels included in the analyses

Accounting for possible misclassification of GM throughout the basal ganglia, we included all voxels of the caudate and lentiform nucleus

(defined with the Wake Forest University (WFU)-Pick Atlas) (Maldjian et al., 2003). Apart from these regions, we included only voxels with a GM value greater than 0.2 (maximum value: 1) and greater than both the WM and CSF value in order to analyze only voxels with sufficient GM and to avoid possible edge effects around the border between GM, WM, and CSF.

Results

GM loss (Fig. 2, blue color; Table 2) was identified bilaterally in the striatum, thalamus, and insula. Further more, dorsolateral frontal regions as well as parietal and occipital regions displayed GM decrease. Accordingly, GM values of all clusters of GM loss were significantly lower in the HD group (2-sided *P* values, <0.001). Moreover, GM values of all clusters of GM loss showed significant interaction of group and age (2-sided *P* values, <0.001).

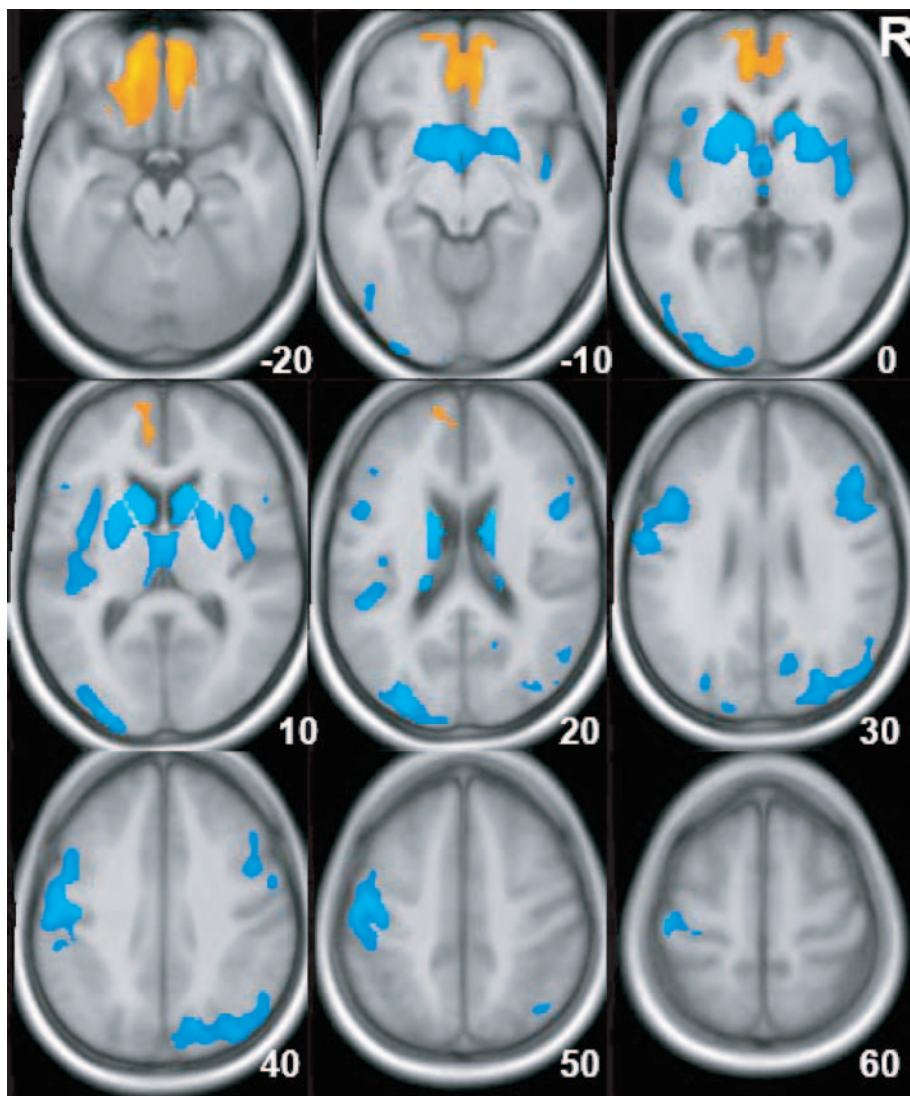


Fig. 2. Grey-matter changes in HD. At a voxel threshold of $P < 0.001$, significant GM changes throughout the whole brain are projected onto the study-specific averaged T1-image (orange color, GM preservation; blue color, GM loss). Increasing significance is color coded from dark to light. The right side of the image shows the right hemisphere. According to the Montreal Neurological Institute (MNI) standard brain, coordinates (Z axis) of axial slices are indicated in the right lower corner of each panel. Only clusters with a peak value of $P < 0.05$ corrected (Friston et al., 1996) and an extent threshold of $P < 0.05$ corrected at the cluster level (18) are shown

Table 2. Areas of grey-matter changes in early Huntington disease

| Cluster size in voxels (1 × 1 × 1 mm) | MNI coordinates | | | Z values of peak voxels | Area |
|--|-----------------|-----|-----|----------------------------|---|
| | x | y | z | | |
| Grey-matter decrease | | | | | |
| 51638 | -11 | 10 | 6 | >7.5 | L caudate body |
| | 15 | 19 | 10 | >7.5 | R caudate body |
| | -15 | 16 | 6 | >7.5 | L caudate head |
| | -18 | 12 | 6 | >7.5 | L putamen |
| | 25 | 7 | 8 | 7.5 | R putamen |
| | -39 | -2 | 11 | 5.0 | L insula |
| | 42 | -10 | -2 | 5.2 | R insula |
| | -2 | -16 | 12 | 4.7 | L thalamus |
| | 3 | -1 | 8 | 4.9 | R thalamus |
| | -3 | 7 | -11 | 5.2 | L ventral striatum/subcallosal area |
| | 15 | 4 | -13 | 5.1 | R ventral striatum/subcallosal area |
| | 48 | 23 | 30 | 5.4 | R frontal lobe, middle frontal g., BA46 |
| | 49 | 10 | 22 | 4.9 | R frontal lobe, inferior frontal g., BA44 |
| | 43 | 10 | 35 | 4.8 | R frontal lobe, middle frontal g., BA9 |
| | 50 | 10 | 28 | 4.8 | R frontal lobe, inferior frontal g., BA9 |
| 16300 | -46 | 13 | 32 | 5.4 | L frontal lobe, middle frontal g., BA9 |
| | -51 | 7 | 23 | 4.5 | L frontal lobe, inferior frontal g., BA44 |
| | -45 | 33 | 15 | 3.2 | L frontal lobe, inferior frontal g., BA46 |
| | -48 | -11 | 46 | 6.1 | L frontal lobe, precentral g., BA4 |
| | -55 | -17 | 42 | 5.9 | L parietal lobe, postcentral g., BA4 |
| | -47 | -31 | 15 | 4.2 | L inferior parietal lobule, BA40 |
| 1265 | -13 | -72 | 26 | 4.9 | L parietal lobe, precuneus, BA31 |
| 9953 | -30 | -90 | 18 | 6.0 | L occ. lobe, middle occ. g., BA19 |
| | -26 | 100 | 1 | 4.5 | L occ. lobe, middle occ. g., BA18 |
| | -14 | -99 | 22 | 4.2 | L occ. lobe, cuneus, BA19 |
| | -48 | -78 | -4 | 3.8 | L occ. lobe, inferior occ. g., BA18 |
| | -47 | -68 | -11 | 3.3 | L occ. lobe, middle occ. g., BA37 |
| 1489 | 15 | -73 | 37 | 5.2 | R parietal lobe, precuneus, BA7 |
| | 28 | -86 | 28 | 4.5 | R occ. lobe, cuneus, BA19 |
| | 51 | -63 | 43 | 4.3 | R inferior parietal lobule, BA40 |
| | 49 | -72 | 35 | 4.0 | R parietal lobe, angular g., BA39 |
| | 39 | -63 | 53 | 4.0 | R superior parietal lobule, BA7 |
| Grey-matter preservation | | | | | |
| 22357 | -13 | 45 | -22 | 6.1 | L frontal lobe, orbital g., BA11 |
| | 8 | 51 | -18 | 4.9 | R frontal lobe, orbital g., BA11 |
| | -5 | 33 | -23 | 4.2 | L frontal lobe, rectal g., BA11 |
| | 9 | 39 | -18 | 5.5 | R frontal lobe, rectal g., BA11 |
| | -6 | 44 | -5 | 4.9 | L anterior cingulate, BA10 |
| | 4 | 44 | -7 | 4.7 | R anterior cingulate, BA10 |
| | -7 | 48 | 9 | 4.0 | L anterior cingulate, BA10 |
| | 17 | 61 | 4 | 4.7 | R medial frontal g., BA10 |
| | -8 | 62 | 13 | 3.8 | L medial frontal g., BA10 |

BA Brodmann area; g. gyrus; L left; occ. occipital; R right.

GM increase (Fig. 2, orange color; Table 2) was identified bilaterally in the anterior cingulate and orbitofrontal cortex of BA 10 and 11 (Z value of peak voxel, 6.1; cluster size at the voxel threshold of $P < 0.001$, 22357 voxels). Direct comparison of absolute GM values derived from this cluster did not reveal significant differences (2-sided P value, >0.2) indicating relative GM preservation rather than absolute GM increase. Interaction analysis of group and

age did not indicate that GM preservation within this area changes in the course of the HD stages under examination (2-sided P value, >0.2).

Discussion

In this study, both GM decrease and increase was investigated in HD. To estimate the influence of disease progression

on the areas identified by our analysis, we performed an interaction analysis of age with group. We decided to perform this interaction analysis since age was closely correlated with motor impairment (Table 1) although this does not certainly imply a similarly close correlation of age with progression of higher cortical function impairment.

GM decrease (Fig. 2, blue color; Table 2) was well in accordance with earlier morphometric studies (Kassubek et al., 2004a, 2005; Peinemann et al., 2005; Rosas et al., 2001, 2002, 2003, 2005). Subcortical GM decrease was pronounced in the dorsal striatum but also found in the ventral striatum and thalamus. At the cortical level, GM loss was found in the insula, in dorsolateral frontal areas as well as in parietal and occipital areas. Since HD is a neurodegenerative disease, we expected GM decrease to progress in the course of the disease. Accordingly, we demonstrated significant interaction of age and group.

In contrast, the anterior cingulate and orbitofrontal cortex displayed GM preservation (Fig. 2, orange color; Table 2). Here the interaction analysis did not indicate changes of GM preservation in the course of the HD stages under examination. Correspondingly, we are not aware of studies that demonstrated involvement of these cortical areas in early HD. However, in one study, serial 11C-raclopride PET scans were performed in 12 patients that, at the first scan, were in later HD stages than our patients. In this study, a decreased 11C-raclopride binding potential (BP) was reported that also reached Brodmann area (BA)10 (Pavese et al., 2003). Moreover, we cannot exclude that, in later stages of HD or in patients with a genetic load higher than that of our HD group, this region might atrophy and, this way, contribute to cognitive and emotional symptoms (Cummings, 1993; Litvan et al., 1998).

The coexistence of GM loss and GM preservation in frontal cortical areas points to differential involvement of these areas in the pathophysiology of HD. Different portions of the frontal lobe are integrated in different circuits that link cortex, basal ganglia and thalamus (Alexander and Crutcher, 1990). Several of these distinct circuits have been described and different distinctions have been made (Alexander and Crutcher, 1990; Joel, 2001). Joel proposed a division of the striatum in 3 “split circuits” (Joel, 2001) each of them involving different frontal areas: 1) the motor circuit includes the primary and supplementary motor cortices that project to the “motor striatum” (i.e., primarily the putamen); 2) within the associative circuit, the dorsolateral prefrontal cortex projects to the “associative striatum” (i.e., primarily the caudate); 3) the limbic circuit comprises the limbic prefrontal cortex and the “limbic (ventral) striatum.” Notably, both areas that displayed GM

preservation in the present study, namely, the orbitofrontal cortex and anterior cingulate, belong to the limbic prefrontal cortex and, hence, to the limbic circuit. In accordance with our data, striatal degeneration is commonly assumed to progress from dorsal to ventral and, probably, from medial to lateral (Fig. 2: color of GM loss, blue; coding of increasing significance, from dark to light) (Vonsattel et al., 1985). Therefore, the primary involvement of the associative circuit and motor circuit as well as the preservation of the limbic circuit has been postulated in early HD (Joel, 2001). However, our data do not simply demonstrate involvement of frontal cortical areas as suggested by the respective part of the striatum (Voorn et al., 2004). Though to different degrees, both the dorsal and ventral striatum show GM loss but frontal cortical areas display inverse changes: whilst areas that are related to the associative and motor circuit display GM loss, parts of the limbic prefrontal cortex resist the process of GM loss in early HD. This differential involvement of frontal cortical areas may rely on interactions between the distinct subcortical frontal circuits. These circuits are not only ‘closed circuits’ but are also interconnected via ‘open pathways’ (Joel, 2001). Theoretically, interconnectivity of subcortical frontal circuits accommodates the coexistence of a variety of symptoms that are related to different circuits but result from damage to only one station of one circuit (Joel, 2001). Therefore cognitive and emotional symptoms could also occur as a result of functional disruptions within the limbic circuit in the absence of GM loss in the limbic prefrontal cortex.

Moreover, another two assumptions are compatible with our data. 1) A compensatory role of the anterior cingulate in early HD has been suggested since HD patients showed an increased activation of the anterior cingulate while learning motor sequences (Rosas et al., 2004). 2) An active role for the generation of “hyperactive behaviors” has been attributed to the orbitofrontal cortex. An “excitatory subcortical output through the medial and orbitofrontal circuits” has been proposed to result in excitatory stimulation of the supplementary motor and premotor cortices (Kulisevsky et al., 2001; Litvan et al., 1998). Accordingly, a projection from the limbic circuit to the motor areas of the motor circuit has been postulated. This “open limbic route” (Joel, 2001) might constitute the neuroanatomical basis of such an excitatory stimulation.

Acknowledgements

We are indebted to Thorleif Etgen who provided most of the data and images of the control group.

References

- Alexander GE, Crutcher MD (1990) Functional architecture of basal ganglia circuits: neural substrates of parallel processing. *Trends Neurosci* 13: 266–271
- Ashburner J, Friston KJ (2000) Voxel-based morphometry – the methods. *Neuroimage* 11: 805–821
- Cummings JL (1993) Frontal-subcortical circuits and human behavior. *Arch Neurol* 50: 873–880
- Folstein MF, Folstein SE, McHugh PR (1975) “Mini-mental state”. A practical method for grading the cognitive state of patients for the clinician. *J Psychiatr Res* 12: 189–198
- Friston KJ, Holmes A, Poline JB, Price CJ, Frith CD (1996) Detecting activations in PET and fMRI: levels of inference and power. *Neuroimage* 4: 223–235
- Gardian G, Vecsei L (2004) Huntington’s disease: pathomechanism and therapeutic perspectives. *J Neural Transm* 111: 1485–1494
- Good CD, Johnsrude IS, Ashburner J, Henson RN, Friston KJ, Frackowiak RS (2001) A voxel-based morphometric study of ageing in 465 normal adult human brains. *Neuroimage* 14: 21–36
- Good CD, Scahill RI, Fox NC, Ashburner J, Friston KJ, Chan D, Crum WR, Rossor MN, Frackowiak RS (2002) Automatic differentiation of anatomical patterns in the human brain: validation with studies of degenerative dementias. *Neuroimage* 17: 29–46
- Graveland GA, Williams RS, DiFiglia M (1985) Evidence for degenerative and regenerative changes in neostriatal spiny neurons in Huntington’s disease. *Science* 227: 770–773
- Huntington’s Disease Collaborative Research Group (1993) A novel gene containing a trinucleotide repeat that is expanded and unstable on Huntington’s disease chromosomes. *Cell* 72: 971–983
- Huntington Study Group (1996) Unified Huntington’s Disease Rating Scale: reliability and consistency. *Mov Disord* 11: 136–142
- Joel D (2001) Open interconnected model of basal ganglia-thalamocortical circuitry and its relevance to the clinical syndrome of Huntington’s disease. *Mov Disord* 16: 407–423
- Kassubek J, Juengling FD, Ecker D, Landwehrmeyer GB (2005) Thalamic atrophy in Huntington’s disease co-varies with cognitive performance: a morphometric MRI analysis. *Cereb Cortex* 15: 846–853
- Kassubek J, Juengling FD, Kioschies T, Henkel K, Karitzky J, Kramer B, Ecker D, Andrich J, Saft C, Kraus P, Aschoff AJ, Ludolph AC, Landwehrmeyer GB (2004b) Topography of cerebral atrophy in early Huntington’s disease: a voxel based morphometric MRI study. *J Neurol Neurosurg Psychiatry* 75: 213–220
- Kassubek J, Landwehrmeyer GB, Ecker D, Juengling FD, Mueche R, Schuller S, Weindl A, Peinemann A (2004a) Global cerebral atrophy in early stages of Huntington’s disease: quantitative MRI study. *Neuroreport* 15: 363–365
- Kulisevsky J, Litvan I, Berthier ML, Pascual-Sedano B, Paulsen JS, Cummings JL (2001) Neuropsychiatric assessment of Gilles de la Tourette patients: comparative study with other hyperkinetic and hypokinetic movement disorders. *Mov Disord* 16: 1098–1104
- Leegwater-Kim J, Cha JH (2004) The paradigm of Huntington’s disease: therapeutic opportunities in neurodegeneration. *NeuroRx* 1: 128–138
- Litvan I, Paulsen JS, Mega MS, Cummings JL (1998) Neuropsychiatric assessment of patients with hyperkinetic and hypokinetic movement disorders. *Arch Neurol* 55: 1313–1319
- Maldjian JA, Laurienti PJ, Kraft RA, Burdette JH (2003) An automated method for neuroanatomic and cytoarchitectonic atlas-based interrogation of fMRI data sets. *Neuroimage* 19: 1233–1239
- Oldfield RC (1971) The assessment and analysis of handedness: the Edinburgh inventory. *Neuropsychologia* 9: 97–113
- Pavese N, Andrews TC, Brooks DJ, Ho AK, Rosser AE, Barker RA, Robbins TW, Sahakian BJ, Dunnett SB, Piccini P (2003) Progressive striatal and cortical dopamine receptor dysfunction in Huntington’s disease: a PET study. *Brain* 126: 1127–1135
- Peinemann A, Schuller S, Pohl C, Jahn T, Weindl A, Kassubek J (2005) Executive dysfunction in early stages of Huntington’s disease is associated with striatal and insular atrophy: A neuropsychological and voxel-based morphometric study. *J Neurol Sci* 239: 11–19
- Rosas HD, Feigin AS, Hersch SM (2004) Using advances in neuroimaging to detect, understand, and monitor disease progression in Huntington’s disease. *NeuroRx* 1: 263–272
- Rosas HD, Goodman J, Chen YI, Jenkins BG, Kennedy DN, Makris N, Patti M, Seidman LJ, Beal MF, Koroshetz WJ (2001) Striatal volume loss in HD as measured by MRI and the influence of CAG repeat. *Neurology* 57: 1025–1028
- Rosas HD, Hevelone ND, Zaleta AK, Greve DN, Salat DH, Fischl B (2005) Regional cortical thinning in preclinical Huntington disease and its relationship to cognition. *Neurology* 65: 745–747
- Rosas HD, Koroshetz WJ, Chen YI, Skeuse C, Vangel M, Cudkovicz ME, Caplan K, Marek K, Seidman LJ, Makris N, Jenkins BG, Goldstein JM (2003) Evidence for more widespread cerebral pathology in early HD: an MRI-based morphometric analysis. *Neurology* 60: 1615–1620
- Rosas HD, Liu AK, Hersch S, Glessner M, Ferrante RJ, Salat DH, van der Kouwe A, Jenkins BG, Dale AM, Fischl B (2002) Regional and progressive thinning of the cortical ribbon in Huntington’s disease. *Neurology* 58: 695–701
- Shoulson I, Fahn S (1979) Huntington disease: clinical care and evaluation. *Neurology* 29: 1–3
- Thieben MJ, Duggins AJ, Good CD, Gomes L, Mahant N, Richards F, McCusker E, Frackowiak RS (2002) The distribution of structural neuropathology in pre-clinical Huntington’s disease. *Brain* 125: 1815–1828
- Vonsattel JP, Myers RH, Stevens TJ, Ferrante RJ, Bird ED, Richardson EP Jr (1985) Neuropathological classification of Huntington’s disease. *J Neuropathol Exp Neurol* 44: 559–577
- Voorn P, Vanderschuren LJ, Groenewegen HJ, Robbins TW, Pennartz CM (2004) Putting a spin on the dorsal-ventral divide of the striatum. *Trends Neurosci* 27: 468–474